

Kinesin-4 functions in vesicular transport on cortical microtubules and regulates cell wall mechanics during cell elongation in plants

Zhaosheng Kong^{1,2}, Motohide Ioki^{1,3}, Siobhan Braybrook⁴, Shundai Li⁵, Zheng-Hua Ye⁶, Yuh-Ru Julie Lee¹, Takashi Hotta^{1,7}, Anny Chang¹, Juan Tian², Guangda Wang², and Bo Liu^{1*}

¹ Department of Plant Biology, University of California, Davis, CA 95616, USA

² State Key Laboratory of Plant Genomics, Institute of Microbiology, Chinese Academy of Sciences, Beijing 100101, China

³ Current address: Center for Environmental Biology and Ecosystem Studies, National Institute for Environmental Studies, Onogawa 16-2, Tsukuba, Ibaraki 305-8506, Japan.

⁴ Sainsbury Laboratory Cambridge, University of Cambridge, Cambridge CB2 1LR, UK

⁵ Department of Biochemistry and Molecular Biology, Pennsylvania State University, State College, PA

⁶ Department of Plant Biology, University of Georgia, Athens, GA

⁷ Current address: Nara Institute of Science and Technology, Graduate School of Biological Sciences, 8916-5 Takayama, Ikoma, Nara 630-0192, Japan

*Author for correspondence. E-mail: bliu@ucdavis.edu Phone: (530) 754-8138

Running title: Kinesin-4 motility and cell elongation

ABSTRACT

In plants, anisotropic cell expansion depends on cortical microtubules that serve as tracks along which macromolecules and vesicles are transported by the motor kinesins of unknown identities. We used cotton (*Gossypium hirsutum*) fibers that underwent robust elongation to discover kinesins that were involved in cell elongation and found GhKinesin-4A expressed abundantly. The motor was detected by immunofluorescence on vesicle-like structures that were associated with cortical microtubules. In *Arabidopsis thaliana*, the orthologous motor At KINESIN-4A/FRA1, previously implicated in cellulose deposition during secondary growth in fiber cells, was examined by live-cell imaging in cells expressing a fluorescently tagged functional protein. The motor decorated vesicle-like particles that exhibit linear movement along cortical microtubules at velocities averaged at 0.89 $\mu\text{m}/\text{min}$, which was significantly different from those linked to cellulose biosynthesis. We also discovered that At KINESIN-4A/FRA1 and the related At Kinesin-4C play redundant roles in cell wall mechanics, cell elongation, and the axial growth of various vegetative and reproductive organs as the loss of At Kinesin-4C greatly enhanced the defects caused by a null mutation at the *Kinesin-4A/FRA1* locus. The double mutant displayed a lack of cell wall softening at normal stages of rapid cell elongation. Furthermore, enhanced deposition of arabinose-

containing carbohydrate was detected in the kinesin-4 mutants. Our findings established a connection between the Kinesin-4-based transport of cargoes containing non-cellulosic components along cortical microtubules and cell wall mechanics and cell elongation in flowering plants.

INTRODUCTION

Plant growth and form are in large the collective result of anisotropic expansion of cells produced earlier by the meristem. Anisotropic growth of plant cells is governed by the cortical microtubules (MTs) that are oriented perpendicularly to the cell expansion axis (Cyr and Palevitz, 1995). Ordered deposition of cellulose microfibrils outside the plasma membrane according to the MT orientation establishes the expansion restriction in that particular dimension (Lloyd and Chan, 2008; Paredez et al., 2006b). The dynamic cortical MT network provides tracks for the traffic of the cellulose synthase (CESA) enzyme and MT-associated CESA compartments (MASCs) (Crowell et al., 2010). In fact, CESA is linked to cortical MTs *via* the CSI1 protein that directly interacts with MTs (Li et al., 2012). However, it is unclear how MASCs interact with MTs and very little if any is known about the exocytotic process dedicated to the delivery of CESA complexes to the plasma membrane.

It is known that perturbations of cellulose biosynthesis by partial loss-of-function mutations often lead to inhibited cell elongation and consequently dwarfism of whole plants (Somerville, 2006). In addition, alteration of the synthesis and deposition of non-cellulosic carbohydrate components also can cause dwarfed growth phenotypes (Atmodjo et al., 2013; Scheller and Ulvskov, 2010). Unlike cellulose that is synthesized by plasma membrane-bound CESA complexes, carbohydrates like hemicellulose and pectin are made in the Golgi apparatus, packaged in vesicles at trans-Golgi network (TGN), and delivered to the plasma membrane *via* exocytosis before being deposited in

the nascent cell wall (Worden et al., 2012). Unfortunately, very little is known about molecular mechanisms that regulate the vesicular transport of these carbohydrates toward the plasma membrane. In particular, it is unclear whether they are transported along cortical MTs by MT-dependent motor proteins.

Unicellular cotton fibers (seed trichomes) grow directionally on the ovule epidermis following pollination. Remarkably, these cells assume diffuse cell expansion for over ten days prior to the initiation of secondary cell wall deposition (Tiwari and Wilkins, 1995). Again, guiding the ordered deposition of cell wall materials is the dynamic MT network, which is organized perpendicularly to the fiber growth axis during the elongation phase (Seagull, 1992). We anticipated that MT-based motor kinesins actively participate in fiber growth and discovered a number of genes encoding kinesins that are abundantly expressed in developing cotton fibers (Lu et al., 2005; Preuss et al., 2003; Preuss et al., 2004). The functions of the motors encoded by orthologous genes can be dissected in the model plant *Arabidopsis thaliana* by examining phenotypes in leaf trichomes, analogous to cotton fibers, exhibited by the corresponding mutants. Interestingly, defects in trichome morphogenesis often are linked to null mutations of such kinesins (Lu et al., 2005; Oppenheimer et al., 1997; Preuss et al., 2003). Further investigations have recovered over a dozen kinesins abundantly expressed during fiber cell elongation in the cotton *Gossypium hirsutum*. Among them, we report here a member of the Kinesin-4 subfamily named Gh KINESIN-4A which shares the highest homology to the FRA1 (fragile fiber 1) protein previously reported in *A. thaliana* (Zhong et al., 2002). FRA1, or At KINESIN-4A, was implied in the deposition and orientation of

cellulose microfibrils during secondary cell wall synthesis in fiber cells in *A. thaliana* (Zhou et al., 2007). However, the *fra1* phenotype in cell elongation indicates that the motor must function during primary cell growth as well. Because the *fra1* mutation does not alter MT organization, it is rather obscure whether At KINESIN-4A/FRA1 acts as a motor for transporting CESA or MASCs or whether the phenotype of misoriented cellulose microfibrils is caused indirectly by defects in non-CESA trafficking events along cortical MTs.

Mutations in the orthologous *Kinesin-4A/BC12* gene in rice also inhibit cell elongation and cause dwarfed growth phenotypes (Li et al., 2011; Zhang et al., 2010), similarly to what is demonstrated by the *fra1* mutation in *A. thaliana*. However, the rice motor was first implicated in cell cycle progression as the *bc12* mutant had reduced number of parenchyma cells in the internode than that in the wild-type (Zhang et al., 2010).

Unexpectedly, the same motor was proposed to bind to the promoter of a gene involved in gibberellic acid (GA) biosynthesis, thus hypothesized to function inside the nucleus (Li et al., 2011). These reports are contradictory to the anticipated typical function of these kinesins as motors for delivering cargoes along MTs in the cytosol. Conventional kinesins carry cargoes and walk along the MT track by using the energy released from ATP hydrolysis after their ATPase activity is activated by MT-binding. Therefore, it is unclear how these kinesins would function inside the nucleus where MTs are absent. Unfortunately, the localization and intracellular motility of the rice or any other plant Kinesin-4 motors have not been examined in live cells so that definite conclusions are yet to be drawn.

Members of the Kinesin-4 subfamily are MT plus end-directed motors that are found in multicellular fungi like *Aspergillus* as well as animals and plants, and in animal cells their functions are mostly linked to mitosis and cytokinesis (Miki et al., 2005; Wickstead and Gull, 2006). Reported Kinesin-4 members typically contain a chromatin-binding site outside their motor domains, and drive chromosome movement along spindle MTs toward their plus ends near the metaphase plate during prometaphase and bind to anti-parallel MTs in the spindle midzone for the establishment of MT-overlapping zone from late anaphase to cytokinesis (Mazumdar and Misteli, 2005). But both the *fra1* mutant and *FRA1/AtKinesin-4A* over-expression plants do not exhibit noticeable phenotypes in mitosis (Zhong et al., 2002; Zhou et al., 2007). Furthermore, outside their motor domains plant Kinesin-4 motors share limited sequence homology with their animal counterparts (Lee and Liu, 2004). Preliminary localization studies showed that At KINESIN-4A/FRA1 primarily appears at the cell cortex in fixed interphase cells (Zhong et al., 2002). Therefore, unlike its animal counterparts, At KINESIN-4A/FRA1 perhaps does not function as a mitotic motor in *A. thaliana*.

In order to determine how the function of Gh KINESIN-4A and At KINESIN-4A/FRA1 is linked to cell elongation, we designed experiments aimed at detecting their intracellular localization and motility in live cells. Expressed in a functional fusion protein of At KINESIN-4A/FRA1 and fluorescent proteins under the native promoter, the motor exhibited motile patterns drastically different from that of the cellulose synthase CESA

or MT polymerization. Our results led us to conclude that At KINESIN-4A/FRA1 functions as a vesicular motor that tracks along cortical MTs for regulating the delivery of non-cellulosic components in the primary cell wall during robust cell expansion. Moreover, we have discovered that among three closely related Kinesin-4 members in *A. thaliana*, At KINESIN-4A/FRA1 and At KINESIN-4C, but not At KINESIN-4B, demonstrated functional redundancy in cell elongation and axial growth across different plant organs.

RESULTS

Comparative Analysis of the Plant Kinesin-4 Motors

The 1033-amino acid cotton Gh KINESIN-4A protein was identified based on a full length cDNA clone isolated from a cDNA library of young cotton fibers (GenBank accession number, KJ701508). Like At KINESIN-4A/FRA1, it contains the motor domain toward the N-terminus and coiled-coil domains occupying large portions outside the motor domain (Figure 1). Such a feature resembles that of the mouse Kinesin-4 motor Mm KIF4. The two plant kinesins share high degrees of homology across the polypeptides (Figure 1). When the two plant kinesins and Mm KIF4 were compared, the homology outside the motor domain dropped significantly (Figure 1).

In the *A. thaliana* genome, there are two more genes that encode Kinesin-4 motors, namely At KINESIN-4B (At3g50240) and At KINESIN-4C (At5g60930). At KINESIN-4A

is more closely related to At KINESIN-4B than to At KINESIN-4C (Richardson et al., 2006). In the model monocot *Oryza sativa* (rice), two Kinesin-4 genes can be found (Guo et al., 2009), one resembling At KINESIN-4A/FRA1 and the other At KINESIN-4C in a phylogenetic analysis using the sequences of the motor domains of Kinesin-4 motors (Supplemental Figure 1A). When sequences outside the motor domains of the three Kinesin-4 motors in *A. thaliana* were compared, in general lower homology was found than the motor domains (Supplemental Figure 1B). Again, the homology of the non-motor sequences between At KINESIN-4A and At KINESIN-4B is higher than that between At KINESIN-4A and At KINESIN-4C.

Gh KINESIN-4A Localizes to Vesicle-like Structures

Because the expression of Gh KINESIN-4A was detected at early stages of cotton fiber elongation, we hypothesized that the motor protein could be detected in fiber cells. In order to do so, we prepared polyclonal antibodies using the polypeptide of amino acids 476-702 of Gh KINESIN-4A as the antigen. Affinity purified antibodies detected a major band at ~116-kDa, which together with degradation products were absent when the antibodies were depleted by the antigen, on SDS-PAGE (Figure 2A). The antibodies were then used for localization of the Gh KINESIN-4A protein in cotton fibers by immunofluorescence. The resulting signals decorated particles that are associated with cortical MTs (Figure 2B, C). This result suggests that Gh KINESIN-4A may be associated with vesicle-like structures at the cell cortex.

Intracellular Motility of At Kinesin-4A

To further elucidate the function of Kinesin-4A in plants, we employed the genetically tractable system of *A. thaliana* in which genetic transformation and live-cell imaging can be done routinely. We tested a number of constructs by transformation into a mutant with a T-DNA insertion at the *Kinesin-4A* locus (*kinesin-4a*) which, due to the loss of its transcript (data not shown), exhibited growth phenotypes resembling those of *fra1* (Zhong et al., 2002). Ultimately we selected a construct expressing the VisGreen-At KINESIN-4A-GFP fusion protein under the native *At KINESIN-4A/FRA1* promoter based on its functionality and visibility by fluorescence microscopy. The fusion protein completely suppressed/complemented the dwarf growth phenotype caused by the *kinesin-4a* mutation (Figure 3A). Multiple transformants exhibited robust growth indistinguishable from the wild-type plant and were subsequently used for imaging the fusion protein in live-cells under a confocal microscope. Based on the functional complementation, we trusted that the motility shown by this fusion protein would represent that of the native motor in cells of *A. thaliana*.

Among cells that exhibited serious elongation defects in the *kinesin-4a* mutant, the epidermal cells at the abaxial surface of the central vein in developing leaves were particularly obvious, concomitant with the severe defect in leaf blade elongation. It suggested the function of the motor there, therefore, we chose to examine these cells. The VisGreen-At KINESIN-4A-GFP signal in cells of the transgenic lines was detected in the cell cortex as particles (Figure 4A-C, Supplemental Movie 1). These particles

often moved in linear tracks that could be revealed by time-averaged/projected image (Figure 4B). Although not all particles decorated by At KINESIN-4A were motile, a significant portion of them demonstrated persistent movement as demonstrated by the Kymograph (Figure 4D).

Because the fluorescent signal of VisGreen-At KINESIN-4A-GFP frequently followed linear tracks, we tested whether the motor followed the tracks of cortical MTs. We adopted the mCherry-TUB6 marker (Nakamura et al., 2010) for observing cortical MTs in these cells. Plants expressing both VisGreen-At KINESIN-4A-GFP and mCherry-TUB6 were selected after crosses. Indeed, the At KINESIN-4A particles were detected on the mCherry-TUB6-labeled MT tracks (Figure 5A, B). When single particles were detected to be associated with MTs, it was found that they often moved along the MT track, and disappeared from the MT focal plane after continuously moving along linear tracks (Figure 5B). This type of processive movements can be clearly demonstrated by Kymographs (Figure 5C).

We quantified the distributions of the velocity frequency and run length demonstrated by the VisGreen-At KINESIN-4A-GFP movement along cortical MTs. The distributions indicated, upon Gaussian fits, that the motor moved at an average velocity of 0.89 $\mu\text{m}/\text{min}$ with an average run length of 1.16 μm ($n=372$) (Figure 6A). Typically, the velocities were within 2 $\mu\text{m}/\text{min}$, suggesting that FRA1 was not a very fast motor *in vivo*, when compared to conventional kinesin in animal cells that move at velocities of a few

micrometers per minute. The run lengths distributed primarily within 2 μm , suggesting that the motor mostly walked long MTs for shorter than 2 min before it fell from the track.

Because it was proposed that At KINESIN-4A/FRA1 might be involved in the motility of CESA enzyme complex, we then examined GFP-CESA3 in similar cells. It was found that GFP-CESA3 demonstrated motilities of an average rate of 0.19 $\mu\text{m}/\text{min}$ (n=214) (Figure 6C), similar to what has been reported in hypocotyl cells previously (Crowell et al., 2009; Paredez et al., 2006a). We further investigated whether the motility of the cellulose synthase complex (CSC) would be affected by the loss of Kinesin-4A. To do so, the YFP-CESA6 fusion protein was expressed in the *kinesin-4a* mutation background. The GFP-CESA6 motility still established linear tracks in the mutant, similarly to what was observed in the control cells (Supplemental Figure 2). We determined that the YFP-CESA6 particles traveled bi-directionally at constant velocities and the velocity distribution for CESA particles was averaged at $213 \pm 45 \text{ nm min}^{-1}$ in the control cells and $196 \pm 90 \text{ nm min}^{-1}$ in *kinesin-4a* mutant cells.

We also tested whether At KINESIN-4A/FRA1 was associated with the CESA-containing SmaCC or MASC structures. When SmaCCs/MASCs, marked by the CESA-interacting protein CSI1 fused with RFP (Li et al., 2012), were detected in cells expressing GFP-KINESIN-4A, the two signals rarely co-localized as 1 out of 66 GFP-KINESIN-4A puncta overlapped with those of RFP-CSI1 (Supplemental Figure 3A). Moreover, the dynamics of GFP-Kinesin-4A was different from that of RFP-CSI1 as

GFP-KINESIN-4A moved much faster and was short-lived (< 5s) (Supplemental Figure 3B). Thus it is unlikely that At KINESIN-4A/FRA1 is responsible for the motility of the CESA enzyme complex or vesicular structures containing CESA because of the discrepancy of localization patterns and velocities. Notably, all these velocities were significantly slower than that of MT polymerization reported by the EB1b-GFP marker at 4.4 $\mu\text{m}/\text{min}$ (n=213) (Figure 6D). Thus we concluded that At KINESIN-4A/FRA1 functions neither in MT polymerization nor in CESA motility.

Retarded Axial Growth and Seed Production in *kinesin-4* Mutants

We hypothesized that the three Kinesin-4 members functioned redundantly for cell elongation in *A. thaliana*. In order to test this hypothesis, we first isolated the *kinesin-4b* and *kinesin-4c* single mutants carrying T-DNA insertions at the corresponding loci. Unlike the *fra1/kinesin-4a* mutant, these two mutants produced plants indistinguishable from the wild-type control (Supplemental Figure 4). This result suggested that Kinesin-4A plays the primary role if the three motors were functionally redundant. We then generated *kinesin-4a; kinesin-4b* and *kinesin-4a; kinesin-4c* double mutants. Because KINESIN-4B shares higher degree of sequence homology to KINESIN-4A than KINESIN-4C, we expected that the *kinesin-4b* would enhance the growth defects caused by *kinesin-4a*. But the *kinesin-4a; kinesin-4b* double mutant resembled the *kinesin-4a* single mutant (Figure 7A-D), further suggesting that At KINESIN-4B does not play a significant role in axial growth in *A. thaliana*. The *kinesin-4a; kinesin-4c* double

mutant, compared to the *kinesin-4a* single mutant, however, exhibited a much higher degree of growth retardation across the entire plant (Figure 7A-D).

One of the most striking phenotypes exhibited by the *kinesin-4a; kinesin-4c* double mutant was the diameter of the seedling rosette prior to inflorescence emergence. While the wild-type leaves expanded rapidly, the double mutant produced significantly smaller seedling rosettes (Figure 7A). The axial growth of leaf blades was severely retarded in the double mutant (Figure 7B).

Because we initially detected this motor in rapidly elongating cotton fibers, we wanted to examine whether trichome growth was affected in the mutant. Both the *kinesin-4a* single and *kinesin-4a; kinesin-4c* double mutants produced trichomes most with three prongs as seen in the wild-type leaf. This result is different from what has been reported for the two other kinesin motors that we identified earlier in cotton fibers, KCBP and KINESIN-13A as the null mutations of the orthologous genes resulted in reduced or enhanced trichome branching in *A. thaliana*, respectively (Lu et al., 2005; Oppenheimer et al., 1997; Preuss et al., 2003). However, we found that the stalk of trichomes was significantly shorter in the *kinesin-4a* mutant than that in the wild-type control and the *kinesin-4c* mutation enhanced this short stalk phenotype (Supplemental Figure 5).

Furthermore, we found that the growth of inflorescence stems was severely affected by the loss of KINESIN-4A, and again the *kinesin-4c* mutation greatly enhanced such phenotypes of dwarfed inflorescence stems (Figure 7D). The organ elongation phenotype was further manifested during silique development, both in terms of the length of siliques and seeds produced per silique (Figure 7E, F). The drastic shortening of the siliques produced by the *kinesin-4a; kinesin-4c* double mutant was concomitant with the reduction of seeds produced in these siliques (Figure 7F).

The *kinesin-4a; kinesin-4c* mutant lacks cell wall elasticity during cell expansion

The localization of KINESIN-4A to cortical MT arrays (Figure 5) and decreased axial growth exhibited by *kinesin-4a; kinesin-4c* double mutants (Figure 7) led us to hypothesize that cell wall mechanics might be altered in the double mutants. To examine this possibility we used Atomic Force Microscopy (AFM) to probe the rigidity of abaxial epidermal cells overlaying the midrib in young leaves (ME cells); these cells showed marked elongation defects in the mutant and were accessible to the method. In 2 week old WT plants, ME cells exhibited an increase in rigidity correlated with age (Figure 8A); the oldest leaf was most rigid while the youngest two leaves were far less rigid along cell walls perpendicular to the surface. This trend was not observed in the *kinesin-4a; kinesin-4c* double mutant ME cells (Figure 8A). ME cells from the *kinesin-4a; kinesin-4c* plants exhibited more rigid perpendicular cell walls in the youngest leaves when compared to WT; the rigidity in double mutant ME cells was almost on par with that of older leaves of WT or *kinesin-4a; kinesin-4c* double mutants. It is interesting to

note that the oldest leaves (Leaf 1) did not show any difference in rigidity between WT and the double mutant. Similar differences in rigidity were observed when all cell wall data was considered from AFM scans (Figure 8B); these data are noisier due to cell length differences and surface geometry (see Materials and Methods).

We reasoned whether the difference in cell wall mechanics between the mutant and control cells was caused by the difference in the carbohydrate composition in the cell wall like cellulose. When the total sugar composition was analyzed, it was found that glucose and most other notable sugar forms did not show obvious difference between the control wild-type sample and *kinesin-4a* single or *kinesin-4a; kinesin-4c* double mutants (Table 1). However the arabinose composition was consistently elevated from $\sim 18 \text{ mg}\cdot\text{g}^{-1}$ in the control to $\sim 28 \text{ mg}\cdot\text{g}^{-1}$ in the mutants (Table 1). This result further indicated that the mutations did not alter the amount of cellulose deposited in the cell wall, but did change non-cellulosic carbohydrates like pectin.

DISCUSSION

In this report, we revealed the intracellular localization and motility of the Kinesin-4A motor in both live-cells in *A. thaliana* and in fixed cotton fibers. Our data suggest that this kinesin motor most likely functions in vesicular transport for non-cellulosic materials during rapid cell elongation. The data also suggest that transport and deposition of non-cellulosic materials during cell elongation are required for robust cell growth.

Furthermore, we found that At KINESIN-4A/FRA1 and At Kinesin-4C motors function

redundantly to support anisotropic cell expansion and axial growth of organs across the entire plant in *A. thaliana*.

Diversified Functions of Kinesin-4 Members

Although the founding member of Kinesin-4, the mouse KIF4 was initially identified as an organelle motor, later studies have drawn our attentions to the functions of this class motors on mitosis (Sekine et al., 1994; Vanneste et al., 2011). Animal Kinesin-4 motors contain chromatin-targeting domains besides having a nuclear localization signal (Vanneste et al., 2011). Such a feature is critical for the motor's function in chromosome congression during prometaphase in order to align them to the metaphase plate.

Besides its function on chromatin, Kinesin-4 motors of animal origins also demonstrate functions on interpolar MTs after anaphase by decorating the MT-overlapping zone (Kurasawa et al., 2004; Zhu and Jiang, 2005). The mouse KIF4 interacts with the MT-cross linker PRC1 (Protein Regulator of Cytokinesis 1) in the MAP65/Ase1 family (Kurasawa et al., 2004). Together, the mouse PRC1 and Kinesin-4 function in establishing a MT-overlapping zone near the MT plus ends and play a critical role in cytokinesis (Bieling et al., 2010b; Subramanian et al., 2013). At KINESIN-4A was detected along cortical MTs in interphase cells but not on chromosomes or mitotic MT arrays during mitosis (data not shown). Thus, we conclude that At KINESIN-4A unlikely bears mitotic functions in *A. thaliana*.

It is noteworthy that the KIF4 kinesin was also demonstrated in the anterograde transport of vesicles in axons (Peretti et al., 2000). Hence, it becomes evident that motors in the Kinesin-4 subfamily have diversified functions, even within a single species.

Kinesin-4 Motility *in vitro* and *in vivo*

The velocity of Kinesin-4 motors has been extensively tested *in vitro*. The founding member of the Kinesin-4 subfamily, KIF4 demonstrates an *in vitro* velocity at ~0.034 $\mu\text{m}/\text{sec}$ or 2.04 $\mu\text{m}/\text{min}$ toward MT plus ends (Sekine et al., 1994). When a fusion protein containing the motor and coiled-coil domains of the At KINESIN-4A/FRA1 (FRA1(707)-GFP) was assayed *in vitro*, it exhibited a higher velocity of 0.4 $\mu\text{m}/\text{sec}$ or 24 $\mu\text{m}/\text{min}$ toward MT plus ends (Zhu and Dixit, 2011). The motors in the subfamily are assumed to bear similar structural features that are supported by the high degree of sequence homology. These two conclusions were drawn based on different approaches that may have contributed to the discrepancies on their motilities when assayed *in vitro*. In fact, the frog Kinesin-4 Xklp1 exhibited drastically faster (~14X) velocity *in vitro* than under the semi *in vivo* conditions when egg extract was used (Bieling et al., 2010a). Such discrepancies between *in vitro* and *in vivo* assays can be found for other kinesins as well (Vanneste et al., 2011). When the motor was reported by a functional full-length fusion protein and assayed *in vivo*, the outcome would comfortably reflect the native scenario.

There is another factor that might have contributed to the disagreement of *in vitro* and *in vivo* results. Autoinhibitory mechanisms are often associated with kinesin motors by having the motor activity inhibited by direct motor-to-tail interactions within the polypeptides (Verhey and Hammond, 2009). In fact, the mammalian Kinesin-4 member Kif12A motor exhibits such an intramolecular autoinhibition mechanism (Cheng et al., 2014). The self-inhibited motors can be activated through cargo binding or phosphorylation in the tail domains, for example (Verhey and Hammond, 2009). It has been demonstrated that the autoinhibition may be attenuated by compromised intramolecular interaction (Cheng et al., 2014). When the truncated version FRA1(707)-GFP was assayed *in vitro* (Zhu and Dixit, 2011), it likely was in an activated state because of lacking the tail domain. This nature might have contributed to the high velocity of the truncated motor and the narrow distribution (homogeneity) of the velocities *in vitro*. A different scenario is expected when the motor is loaded with its cargo. Under working conditions *in vivo*, At KINESIN-4A/FRA1 would be present in both inactive as well as partially and fully active forms, depending on their status of cargo binding. In addition, cytosolic viscosity might have also slowed down of the motor under working conditions. Consequently, they would display a relatively wide range of velocities in addition to some being immobile.

Collectively, we conclude that At KINESIN-4A/FRA1 is rather a slow motor when compared to the conventional kinesin. However, it unlikely serves as a motor for

transporting CESA-rich vesicles described as small CESA compartments or microtubule-associated cellulose synthase compartment which are tethered on depolymerizing MTs (Gutierrez et al., 2009), because the At Kinesin-4A/FRA1 velocity is fast and not steady and their trajectory is non-linear. In fact, it has been concluded that the slow movement of CESA enzymes on cortical MTs is unlikely driven by kinesins (Paredes et al., 2006a). In contrast, motile At KINESIN-4A/FRA1 motors mostly run at a steady-rate along a linear trajectory as revealed by Kymograph (See Figure 5). Thus we conclude that At KINESIN-4A/FRA1 exhibits a novel type of motility along cortical MTs in actively elongating plant cells.

It is intriguing what the cargo(s) of the plant KINESIN-4A motor are. After ruling out CESA or its related compartments, we speculate that it may be involved in delivering membranous compartments containing non-cellulosic carbohydrate components for cell wall synthesis.

Plant Kinesin-4 and Primary Cell Growth/Elongation

The previous *in vivo* analysis of the *fra1* mutant has indicated that At KINESIN-4A/FRA1 is involved in the cellulose deposition during secondary cell wall thickening although the mutant shows normal cellulose contents in the cell wall (Zhong et al., 2002).

Surprisingly, over expression of the motor causes severe reduction of the thickness of the secondary cell wall in fiber cells (Zhou et al., 2007). Interestingly, the motor is expressed not only in cells undergoing secondary growth but also in the meristem as

well as in parenchyma cells (Zhou et al., 2007). Our AFM-based examinations revealed abnormal cell wall mechanics in the epidermal cells of unexpanded leaves in the *kinesin-4a; kinesin-4c* double mutant. In the wild-type leaves, these cells would undergo rapid and robust expansion, concomitant with softening decreases in cell wall rigidity. Our data indicated a lack of softening in the double mutant during expansion, that was consistent with the small leaf size and curling morphology. The rigid cell wall phenotype at early stages of cell elongation is likely associated with the *kinesin-4a* mutation and enhanced by the *kinesin-4c* mutation. Together with the fact that the cotton ortholog is abundantly expressed during fiber elongation stages, these lines of evidence further support the function of At KINESIN-4A/FRA1 during primary cell elongation.

In general, we often focus on cellulose deposition when primary cell elongation is examined. Undoubtedly, compromised cellulose synthesis by mutations in the CESA genes causes defective cell elongation (Beeckman et al., 2002). In the cell wall, cellulose microfibrils are spaced by matrix components like non-cellulosic complex carbohydrates or proteinaceous components. Hemicelluloses directly contribute to the strength of the plant cell wall by cross-linking cellulose microfibrils (Scheller and Ulvskov, 2010). For example, defects in the biosynthesis of the hemicellulose glucuronoxylan cause severe seedling dwarfism (Wu et al., 2010), somewhat similar to what *kinesin-4a/fra1* mutants behave. Although the significance of their proper addition to the nascent cell wall is widely recognized (Hayashi and Kaida, 2011), it is unclear how their deposition is coordinated with that of cellulose and how cell wall remodeling is taking

place after complex carbohydrates are deposited. We know very little if any about how hemicelluloses and pectin are delivered by exocytosis after being packaged at TGN. In addition, vesicles from TGN may contain enzymes that function in softening cellulose microfibrils in the nascent cell wall during rapid expansion. It is proposed here that these vesicles may be transported along cortical MTs by kinesin motors like KINESIN-4A/C during rapid elongation of plant cells. Improper deposition of non-cellulosic carbohydrates in the cell wall may have altered the deposition and/or organization of cellulose microfibrils. This notion is consistent with the observed aberrantly oriented cellulose microfibrils in the *fra1* mutant cells (Zhong et al., 2002). Consequently, the stems of the *fra1* mutant become fragile. Therefore, we suggest that orchestrated deposition of components like pectin and hemicelluloses would directly influence the outcome of cell elongation and *vice versa*. In fact, it has been documented that a reduction in one cell wall component may cause a compensatory increase in another cell wall component. For example, pectin content is significantly elevated in two cellulose deficient *kor* and *prc1* mutants (Fagard et al., 2000; His et al., 2001).

Our results further suggest that orchestrated secretion of non-cellulosic carbohydrates to the cell wall also is critical for cell wall mechanics. For example, arabinose is abundantly found in pectin deposited in the middle lamella. Pectin is often linked to xyloglucan prior to secretion (Popper and Fry, 2008). The loss of the Kinesin-4 motor somehow might have altered modification of arabinose-containing carbohydrates so that pectin and hemicellulose would contain more arabinose. Consequently, such changes might result in reduced elasticity of the cell wall prior to elongation as observed here.

In summary, in this study we detected At KINESIN-4A/FRA1 along cortical MTs. Our results support the notion that the kinesin likely acts as a long expected motor for vesicle transport in rapidly elongating plant cells. This finding inspires us to search for protein(s) that allow the loading of vesicles to the Kinesin-4 motor in higher plant cells that undergo rapid elongation.

MATERIALS AND METHODS

Plant Materials and Growth Conditions

The cotton *G. hirsutum* plants were grown under the greenhouse condition in Davis, CA. The *A. thaliana* plants were grown under controlled conditions as described previously (Kong et al., 2010; Lee et al., 2007). T-DNA insertion lines SALK_084463, SALK_022231, and SALK_124215 at the *Kinesin-4A/FRA1*, *Kinesin-4B*, and *Kinesin-4C* loci were acquired from the Arabidopsis Biological Research Center at the Ohio State University. Standard genetic crosses were carried out between mutants and wild-type plants and among the mutant lines. The marker lines expressing mCherry-TUB6, EB1b-GFP, and GFP-CESA3 (Crowell et al., 2009; Dixit et al., 2006; Nakamura et al., 2010) were generously provided by the corresponding colleagues.

Isolation of the *Gh Kinesin-4A* cDNA

A full-length cDNA clone of Gh KINESIN-4A was isolated from a cotton fiber specific cDNA library (Pear et al., 1996), using a similar approach as described in one of our previous reports (Preuss et al., 2004). The cDNA clone was subsequently sequenced at a commercial DNA sequencing facility. The GenBank accession number if GhKinesin-4A is KJ701508.

Detection and Verification of the T-DNA Insertions

Standard polymerase chain reaction (PCR)-based method was applied to detect the reported T-DNA insertions according to an established protocol (Krysan et al., 1999). The T-DNA specific primer is LBa1 5'-TGGTTCACGTAGTGGGCCATCG-3' for the SALK lines used in this study. Gene specific primers include 84463LP 5'-ATTTGCTCCACGGTGATAGTG-3' and 84463RP 5'-TCGCGACGTTTTTAGAATCAG-3' for *SALK_084463* of *Kinesin-4A*; 22231LP 5'-CATAGGTGCAAATGGGAACAC-3' and 22231RP 5'-AACATGTGCACCTTCTTTTCG-3' for *SALK_022231* of *Kinesin-4B*; and 124215LP 5'-GCCATGAGTTTGTGCATCTC-3' and 124215RP 5'-TGCTCACTTCAAGAAAAGTTGG-3' for *SALK_124215* of *Kinesin-4C*. The *kinesin-4a*, *kinesin-4b*, and *kinesin-4c* mutations were detected by using primer combinations of LBa1 and 84463RP, 22231RP, or 124215RP, respectively.

Genetic Suppression/Complementation of the *kinesin-4a* Mutation

The genomic fragment of the *At Kinesin4A* gene included its coding sequence and the 1828 bp upstream fragments from the initiation ATG and was amplified from a genomic DNA preparation by PCR using the Phusion DNA polymerase (New England Biolabs). The primers were 47820P-F (5'-CACCTCATAGAAATCAATCTCTCGTAGATCAGTGATCAC-3', 5'-CACC, underlined, is for directional cloning) and GA-47820-R (5'-TGCGCCTGCGCCCATGATCTTATTAGGTAGAGCCTTAAGTCG-3', the 12bp fragment, underlined, encodes a "Glycine-Alanine" duplicates linker between AtKinesin4A and FLAG to facilitate functional fusion). The amplified fragment was cloned into the pENTR vector by a TOPO based cloning strategy according to manufacturer's instruction (Invitrogen). In addition, a VisGreen GFP (Teerawanichpan et al., 2007) fusion was added to the N-terminus of the AtKinesin4A protein by the following manipulation. The promoter region of the *AtKinesin4A* gene was amplified by primers of 47820P-F and 47820P-R (5'-GCCCTTGCTCACCAATTGGAAGAAGAAGAAGTAATCTAGAATCG-3', the 15-bp fragment underlined is the reverse complement sequence of the first 15-bp of coding sequence of *AtKinesin4A* to provide an overlap for subsequent fusion PCR). The VisGreen-coding sequence was amplified by primers of VisGreen-F (5'-CTTCTTCTTCTTCCAATGGTGAGCAAGGGCGAGGAGC-3', the 15 bp fragment underlined is the last 15 bp in front of initiation ATG of *AtKinesin4A* to provide an overlap for subsequent fusion PCR) and VisGreen-R (5'-CCGCTCGAGCTTGTACAGCTCGTCCATGCCGTGAG-3', Xho I site underlined, the lower-case overhang was added for effective digestion reaction). The PCR fragments of promoter region and VisGreen was linked by fusion PCR using Phusion DNA

polymerase (Thermo Fisher), modified from a published protocol (Szewczyk et al., 2006). The resulting fusion fragment was cloned into the pENTR vector by a TOPO based cloning to get the Entry 1 clone. The *AtKinesin4A* coding sequence was amplified by 47820-F (5'-
CACCCTCGAGGGCGCAGGCGCAATGGAATCTACGCCGCCACCGGATG-3', the 5' end CACC is for directional cloning, the italic is Xho I site, and the underlined 12bp fragment encodes a "Glycine-Alanine" duplicates linker between VisGreen and AtKinesin4A to facilitate functional fusion) and GA-47820-R (5'-
TGCGCCTGCGCCCATGATCTTATTAGGTAGAGCCTTAAGTCG-3', the 12bp fragment, underlined, encodes a "GlycineAlanine" duplicates linker between AtKinesin4A and GFP to facilitate functional fusion). The resulting fragment cloned into the pENTR vector by a TOPO based cloning to get the Entry 2 clone. Both the Entry 1 vector and Entry 2 vector were digested by Not I and Xho I, further ligation reaction was conducted between the Gel purified fragment containing promoter and VisGreen and the fragment containing the coding sequence of *AtKinesin4A*. Finally, the resulting Entry 3 clone was delivered into pGWB4 (Nakagawa et al., 2007) by recombination reaction to get *P_{Kinesin4A}::VisGreen-Kinesin4A-GFP* construct. The resulting plasmids were transformed into the agrobacteria GV3101, followed by transformation into *A. thaliana* according to the standard floral dipping protocol (Clough and Bent, 1998).

Production of Anti-Gh Kinesin-4A Antibodies and Immunolocalization

A cDNA fragment encoding polypeptide of amino acids 476-702 in Gh Kinesin-4A was amplified using the primers of 5'-CACCGAGGTGATTCCAGAGAAATTGAG-3' and 5'-ATTGTCGACGAGCAGCAGATTTACGAGCT-3'. The resulting fragment was cloned into the pGEX-KG vector (Guan and Dixon, 1991) at the EcoRI and Sall sites. Consequently, a GST fusion protein was expressed in bacteria and purified before being used as an antigen for immunization in two rabbits. Specific antibodies were purified as described previously (Preuss et al., 2004).

Cotton fibers were collected from growing cotton bolls and fixed for immunolocalization as we have done for other motors (Preuss et al., 2004). Besides the anti-Gh Kinesin-4A antibodies, the DM1A anti-tubulin antibody (Sigma) was used to label MTs. The secondary antibodies used in this study are FITC-conjugated donkey anti-rabbit IgG, and Texas Red-conjugated donkey anti-mouse IgG (Rockland Immunochemicals). In the control experiment, antibodies were pre-absorbed with the antigen prior to their application.

Fluorescent Microscopy and Digital Imaging

Cotton fibers were fixed and processed for immunolocalization as described previously (Preuss et al., 2003). Stained fiber cells were observed under an Eclipse 600 fluorescent microscope (Nikon).

Live cell imaging of VisGreen-At KINESIN-4A-GFP was carried out under a spinning disk confocal microscope equipped with lasers for GFP and mCherry (Intelligent Design), as described previously (Hotta et al., 2012). Time-lapsed images were further processed in the Metamorph software package (Molecular Devices) for analysis of motility using the Kymograph tool. The run length distribution of VisGreen-AtKinesin4A-GFP and the velocity distribution of VisGreen-At KINESIN-4A-GFP, GFP-CESA3 and EB1b-GFP were calculated in Origin software (Origin Lab) by frequency counts. Histograms of run length and velocity distribution of VisGreen-AtKinesin4A-GFP were fitted by a quick fit method in Origin using the function of ExpDecay with offset. Histograms of velocity distribution of GFP-CESA3 and EB1b-GFP were fitted using the Gauss Function $y = y_0 + Ae^{-\frac{(x-x_c)^2}{2w^2}}$ in Origin. The mean values and 95% confidence interval were calculated in SAS (SAS software).

To observe YFP-CESA6/RFP-TUA5 in the *kinesin-4a* mutation (SALK_084463) background, a standard genetic cross was made between the mutant and YFP-CESA6 plus RFP-TUA5 reporter line (Lei et al., 2013). Fluorescent signals were observed under a Yokogawa CSUX1 spinning disk confocal system operated by the Metamorph software (Molecular Devices), followed by image and particle analyses via the ImageJ and Imaris (Bitplane) software packages, as described previously (Bashline et al., 2013).

Atomic force microscopy (AFM) - based nanoindentation

AFM - based nanoindentation was performed as follows, according to published studies (Braybrook and Peaucelle, 2013; Peaucelle et al., 2011). WT (Col) and *kinesin-4a*; *kinesin-4c* double mutant seedlings were grown on standard media (1/2MS, 1g/L sucrose, MES pH 5.7, B-vitamins, 0.7% agar) in long day conditions at 20°C for 2 weeks. At the 2 week mark, seedlings were removed from media and leaves dissected from the plant; at this time all plants had roughly 4 dissectible leaves, with 1-2 more small leaves that were not easily dissected (Supplemental Figure 6). Dissectible leaves were further cut to allow a flat abaxial area to be presented upwards (Supplemental Figure 6). These cut areas were fixed to a glass slide using 1% low melt agarose made in 0.55M mannitol. A sealing ring was placed around the mounted tissue samples and filled with 0.55M mannitol to plasmolyze cells. Samples were set to plasmolyze for 15-30 minutes and then mounted under a JPK NanoWizard 3 AFM (JPK, Berlin, DE). AFM-based nanoindentations were performed with a 1µm diameter rounded pyramidal tip attached to a cantilever of 42.859 N/m (Windsor Scientific, Slough, UK). The same cantilever was used for all samples and was calibrated using thermal tuning. Before each experiment the sensitivity of the cantilever was determined by indentation on glass. Indentations were performed in grids of 32x32 points over 100µm x 50µm areas (Supplemental Figure 6), at a force of 500 nN which yielded an average indentation depth of 250 nm on perpendicular to surface cell walls and 500nm on parallel walls. Apparent Young's moduli (EA) were calculated using JPK Data Processing Software (v. spm-4.3-41; JPK, Berlin, DE) using experimentally determined sensitivity and cantilever spring constants, and spherical tip geometry. Reported EA values are taken from indentation curves. Sample numbers: WT Leaf 1, n=3; WT Leaf 3, n=3; WT Leaf 4, n=3;

kinesin-4a; kinesin-4c Leaf 1 n=3; *kinesin-4a; kinesin-4c* Leaf 3 n=4; *kinesin-4a; kinesin-4c* Leaf 4 n=4. Data in 'perpendicular wall' box plots correspond to bulked EA values from perpendicular walls, 20 values per sample. All data correspond to the following number of bulked EA values: WT Leaf 1 n=3072; WT Leaf 3 n=3072; WT Leaf 4 n=3072; *kinesin-4a; kinesin-4c* Leaf 1 n=4096; *kinesin-4a; kinesin-4c* Leaf 3 n=4096; *kinesin-4a; kinesin-4c* Leaf 4 n= 4096. Data was graphed in MATLAB using the Violin.m package, and t-tests were performed therein as well.

Cell wall composition analysis

Mature inflorescence stems of wild type and mutants were collected and ground into fine powder in liquid nitrogen with a mortar and pestle. The ground material was homogenized in 70% and 100% (v/v) ethanol using a Polytron homogenizer and further extracted with methanol:chloroform (1:1, v/v) and acetone. The resulting cell wall residues were dried in a vacuum oven and used for analysis of total sugar composition. Cell wall sugars (as alditol acetates) were determined following the procedure described by (Hoebler et al., 1989). Sugars were analyzed using a Perkin–Elmer Clarus 500 gas–liquid chromatograph instrument equipped with a 30 m x 0.25 mm (i.d.) silica capillary column DB 225 (Alltech Associates). Two biological replicates for wild type and mutants were used for cell wall sugar analysis and each sample was run in duplicate.

Accession Numbers

The Arabidopsis Information Resource (TAIR) locus identifiers for the genes mentioned in this study are At5g47820 for At KINESIN-4A/FRA1, At3g50240 for At KINESIN-4B, and At5g60930 for At KINESIN-4C. The GenBank accession number of the Gh KINESIN-4A cDNA sequence is KJ701508.

ACKNOWLEDGEMENTS

We thank Richard Cyr at Pennsylvania State University, Takashi Hashimoto at the Nara Institute of Science and Technology in Japan, Gopalan Selvaraj at the Plant Biotechnology Institute of the National Research Council of Canada, and Samantha Vernhettes at Institut Jean-Pierre Bourgin of INRA in France for generously providing the marker lines used here, Tsuyoshi Nakagawa at Shimane University in Japan for the pGWB vectors, and the Arabidopsis Biological Resource Center at Ohio State University for distributing the T-DNA lines used in this study. We also want to thank Ms. Lei Lei for her assistance in data analysis and figure preparation. This report is based on work supported by the National Science Foundation under grant MCB-1243959 (BL and YRJL), Physical Biosciences Program of the Office of Basic Energy Sciences of the U.S. Department of Energy under the contracts DE-FG02-04ER15554 (BL) and DE-FG02-03ER15415 (Z-HY). SL is supported by the Center for LignoCellulose Structure and Formation, an Energy Frontier Research Center funded by the U.S. Department of Energy under the award DE-SC0001090 and SAB is supported by a Gatsby Foundation Fellowship. Any opinions, findings, and conclusions or recommendations expressed in

this article are those of the authors and do not necessarily reflect the views of the funding agencies.

Table 1. Cell wall composition in wild-type (WT) and *kinesin-4* mutants (mg g⁻¹ cell wall)

| Sample | Xylose | Glucose | Mannose | Galactose | Arabinose | Rhamnose | Fucose |
|---|---------------|----------------|----------------|------------------|------------------|-----------------|---------------|
| WT | 71.2±7.0 | 270.0±44.7 | 13.6±1.4 | 23.3±1.6 | 18.3±0.3 | 13.1±0.2 | 3.5±2.3 |
| <i>kinesin-4a</i> | 72.6±8.7 | 272.4±22.9 | 16.9±1.3 | 31.3±1.8 | 28.8±2.3 | 14.5±1.2 | 1.4±0.4 |
| <i>kinesin-4a;</i> <i>kinesin-4c</i> | 73.5±4.3 | 243.0±25.3 | 14.3±0.7 | 26.2±1.8 | 28.1±1.4 | 11.8±0.9 | 1.5±0.5 |

REFERENCES

- Atmodjo, M.A., Hao, Z., and Mohnen, D. (2013). Evolving views of pectin biosynthesis. *Annu Rev Plant Biol* 64:747-779.
- Bashline, L., Li, S., Anderson, C.T., Lei, L., and Gu, Y. (2013). The endocytosis of cellulose synthase in *Arabidopsis* is dependent on mu2, a clathrin-mediated endocytosis adaptin. *Plant Physiol* 163:150-160.
- Beeckman, T., et al. (2002). Genetic complexity of cellulose synthase a gene function in *Arabidopsis* embryogenesis. *Plant Physiol* 130:1883-1893.
- Bieling, P., Kronja, I., and Surrey, T. (2010a). Microtubule motility on reconstituted meiotic chromatin. *Curr Biol* 20:763-769.
- Bieling, P., Telley, I.A., and Surrey, T. (2010b). A minimal midzone protein module controls formation and length of antiparallel microtubule overlaps. *Cell* 142:420-432.
- Braybrook, S.A., and Peaucelle, A. (2013). Mechano-chemical aspects of organ formation in *Arabidopsis thaliana*: the relationship between auxin and pectin. *PLoS One* 8:e57813.
- Cheng, L., et al. (2014). Human CFEOM1 mutations attenuate KIF21A autoinhibition and cause oculomotor axon stalling. *Neuron* 82:334-349.
- Clough, S.J., and Bent, A.F. (1998). Floral dip: a simplified method for *Agrobacterium*-mediated transformation of *Arabidopsis thaliana*. *Plant J* 16:735-743.
- Crowell, E.F., et al. (2009). Pausing of Golgi bodies on microtubules regulates secretion of cellulose synthase complexes in *Arabidopsis*. *Plant Cell* 21:1141-1154.
- Crowell, E.F., Gonneau, M., Stierhof, Y.D., Hofte, H., and Vernhettes, S. (2010). Regulated trafficking of cellulose synthases. *Curr Opin Plant Biol* 13:700-705.
- Cyr, R.J., and Palevitz, B.A. (1995). Organization of cortical microtubules in plant cells. *Curr Opin Cell Biol* 7:65-71.
- Dixit, R., Chang, E., and Cyr, R. (2006). Establishment of polarity during organization of the acentrosomal plant cortical microtubule array. *Mol Biol Cell* 17:1298-1305.
- Fagard, M., et al. (2000). PROCUSTE1 encodes a cellulose synthase required for normal cell elongation specifically in roots and dark-grown hypocotyls of *Arabidopsis*. *Plant Cell* 12:2409-2424.
- Guan, K.L., and Dixon, J.E. (1991). Eukaryotic proteins expressed in *Escherichia coli*: an improved thrombin cleavage and purification procedure of fusion proteins with glutathione S-transferase. *Anal Biochem* 192:262-267.
- Guo, L., Ho, C.-M.K., Kong, Z., Lee, Y.-R.J., Qian, Q., and Liu, B. (2009). Evaluating the microtubule cytoskeleton and its interacting proteins in monocots by mining the rice genome. *Ann Bot* 103:387-402.
- Gutierrez, R., Lindeboom, J.J., Paredes, A.R., Emons, A.M., and Ehrhardt, D.W. (2009). *Arabidopsis* cortical microtubules position cellulose synthase delivery to the plasma membrane and interact with cellulose synthase trafficking compartments. *Nat Cell Biol* 11:797-806.
- Hayashi, T., and Kaida, R. (2011). Functions of xyloglucan in plant cells. *Mol Plant* 4:17-24.
- His, I., Driouch, A., Nicol, F., Jauneau, A., and Hofte, H. (2001). Altered pectin composition in primary cell walls of korrigan, a dwarf mutant of *Arabidopsis* deficient in a membrane-bound endo-1,4-beta-glucanase. *Planta* 212:348-358.
- Hoebler, C., Barry, J.L., David, A., and Delort-Laval, J. (1989). Rapid acid hydrolysis of plant cell wall polysaccharides and simplified quantitative determination of their neutral monosaccharides by gas-liquid chromatography. *J. Agric. Food Chem.* 37:360-367.

- Hotta, T., et al. (2012). Characterization of the Arabidopsis augmin complex uncovers its critical function in the assembly of the acentrosomal spindle and phragmoplast microtubule arrays. *Plant Cell* 24:1494-1509.
- Kong, Z., Hotta, T., Lee, Y.R., Horio, T., and Liu, B. (2010). The γ -tubulin complex protein GCP4 is required for organizing functional microtubule arrays in Arabidopsis thaliana. *Plant Cell* 22:191-204.
- Krysan, P.J., Young, J.C., and Sussman, M.R. (1999). T-DNA as an insertional mutagen in Arabidopsis. *Plant Cell* 11:2283-2290.
- Kurasawa, Y., Earnshaw, W.C., Mochizuki, Y., Dohmae, N., and Todokoro, K. (2004). Essential roles of KIF4 and its binding partner PRC1 in organized central spindle midzone formation. *EMBO J* 23:3237-3248.
- Lee, Y.R.J., Li, Y., and Liu, B. (2007). Two Arabidopsis phragmoplast-associated kinesins play a critical role in cytokinesis during male gametogenesis. *Plant Cell* 19:2595-2605.
- Lee, Y.R.J., and Liu, B. (2004). Cytoskeletal motors in Arabidopsis. Sixty-one kinesins and seventeen myosins. *Plant Physiol* 136:3877-3883.
- Lei, L., Li, S., Du, J., Bashline, L., and Gu, Y. (2013). Cellulose synthase INTERACTIVE3 regulates cellulose biosynthesis in both a microtubule-dependent and microtubule-independent manner in Arabidopsis. *Plant Cell* 25:4912-4923.
- Li, J., et al. (2011). Mutation of rice *BC12/GDD1*, which encodes a kinesin-like protein that binds to a GA biosynthesis gene promoter, leads to dwarfism with impaired cell elongation. *Plant Cell* 23:628-640.
- Li, S., Lei, L., Somerville, C.R., and Gu, Y. (2012). Cellulose synthase interactive protein 1 (CSI1) links microtubules and cellulose synthase complexes. *Proc Natl Acad Sci U S A* 109:185-190.
- Lloyd, C., and Chan, J. (2008). The parallel lives of microtubules and cellulose microfibrils. *Curr Opin Plant Biol* 11:641-646.
- Lu, L., Lee, Y.R., Pan, R., Maloof, J.N., and Liu, B. (2005). An internal motor kinesin is associated with the Golgi apparatus and plays a role in trichome morphogenesis in Arabidopsis. *Mol Biol Cell* 16:811-823.
- Mazumdar, M., and Misteli, T. (2005). Chromokinesins: multitasking players in mitosis. *Trends Cell Biol* 15:349-355.
- Miki, H., Okada, Y., and Hirokawa, N. (2005). Analysis of the kinesin superfamily: insights into structure and function. *Trends Cell Biol* 15:467-476.
- Nakagawa, T., et al. (2007). Development of series of gateway binary vectors, pGWBs, for realizing efficient construction of fusion genes for plant transformation. *J Biosci Bioeng* 104:34-41.
- Nakamura, M., Ehrhardt, D.W., and Hashimoto, T. (2010). Microtubule and katanin-dependent dynamics of microtubule nucleation complexes in the acentrosomal Arabidopsis cortical array. *Nat Cell Biol* 12:1064-1070.
- Oppenheimer, D.G., et al. (1997). Essential role of a kinesin-like protein in Arabidopsis trichome morphogenesis. *Proc Natl Acad Sci USA* 94:6261-6266.
- Paredes, A.R., Somerville, C.R., and Ehrhardt, D.W. (2006a). Visualization of cellulose synthase demonstrates functional association with microtubules. *Science* 312:1491-1495.
- Paredes, A.R., Wright, A., and Ehrhardt, D.W. (2006b). Microtubule cortical array organization and plant cell morphogenesis. *Current Opinion in Plant Biology* 9:571-578.
- Pear, J.R., Kawagoe, Y., Schreckengost, W.E., Delmer, D.P., and Stalker, D.M. (1996). Higher plants contain homologs of the bacterial *celA* genes encoding the catalytic subunit of cellulose synthase. *Proc Natl Acad Sci USA* 93:12637-12642.
- Peaucelle, A., Braybrook, S.A., Le Guillou, L., Bron, E., Kuhlemeier, C., and Hofte, H. (2011). Pectin-induced changes in cell wall mechanics underlie organ initiation in Arabidopsis. *Curr Biol* 21:1720-1726.

- Peretti, D., Peris, L., Rosso, S., Quiroga, S., and Caceres, A. (2000). Evidence for the involvement of KIF4 in the anterograde transport of L1-containing vesicles. *Journal of Cell Biology* 149:141-152.
- Popper, Z.A., and Fry, S.C. (2008). Xyloglucan-pectin linkages are formed intra-protoplasmically, contribute to wall-assembly, and remain stable in the cell wall. *Planta* 227:781-794.
- Preuss, M.L., Delmer, D.P., and Liu, B. (2003). The cotton kinesin-like calmodulin-binding protein associates with cortical microtubules in cotton fibers. *Plant Physiol* 132:154-160.
- Preuss, M.L., Kovar, D.R., Lee, Y.-R.J., Staiger, C.J., Delmer, D.P., and Liu, B. (2004). A plant-specific kinesin binds to actin microfilaments and interacts with cortical microtubules in cotton fibers. *Plant Physiol* 136:3945-3955.
- Richardson, D.N., Simmons, M.P., and Reddy, A.S. (2006). Comprehensive comparative analysis of kinesins in photosynthetic eukaryotes. *BMC Genomics* 7:18.
- Scheller, H.V., and Ulvskov, P. (2010). Hemicelluloses. *Annu Rev Plant Biol* 61:263-289.
- Seagull, R.W. (1992). A quantitative electron microscopic study of changes in microtubule arrays and wall microfibril orientation during in-vitro cotton fiber development. *J Cell Sci* 101:561-577.
- Sekine, Y., et al. (1994). A novel microtubule-based motor protein (KIF4) for organelle transports, whose expression is regulated developmentally. *J Cell Biol* 127:187-201.
- Somerville, C.R. (2006). Cellulose synthesis in higher plants. *Annu Rev Cell Dev Biol* 22:53-78.
- Subramanian, R., Ti, S.C., Tan, L., Darst, S.A., and Kapoor, T.M. (2013). Marking and measuring single microtubules by PRC1 and kinesin-4. *Cell* 154:377-390.
- Szewczyk, E., et al. (2006). Fusion PCR and gene targeting in *Aspergillus nidulans*. *Nat Protoc* 1:3111-3120.
- Teerawanichpan, P., Hoffman, T., Ashe, P., Datla, R., and Selvaraj, G. (2007). Investigations of combinations of mutations in the jellyfish green fluorescent protein (GFP) that afford brighter fluorescence, and use of a version (VisGreen) in plant, bacterial, and animal cells. *Biochim Biophys Acta* 1770:1360-1368.
- Tiwari, S.C., and Wilkins, T.A. (1995). Cotton (*Gossypium hirsutum*) seed trichomes expand via diffuse growing mechanism. *Canadian Journal of Botany* 73:746-757.
- Vanneste, D., Ferreira, V., and Vernos, I. (2011). Chromokinesins: localization-dependent functions and regulation during cell division. *Biochem Soc Trans* 39:1154-1160.
- Verhey, K.J., and Hammond, J.W. (2009). Traffic control: regulation of kinesin motors. *Nat Rev Mol Cell Biol* 10:765-777.
- Wickstead, B., and Gull, K. (2006). A "holistic" kinesin phylogeny reveals new kinesin families and predicts protein functions. *Mol Biol Cell* 17:1734-1743.
- Worden, N., Park, E., and Drakakaki, G. (2012). Trans-Golgi network: an intersection of trafficking cell wall components. *J Integr Plant Biol* 54:875-886.
- Wu, A.M., et al. (2010). Analysis of the Arabidopsis IRX9/IRX9-L and IRX14/IRX14-L pairs of glycosyltransferase genes reveals critical contributions to biosynthesis of the hemicellulose glucuronoxylan. *Plant Physiol* 153:542-554.
- Zhang, M., et al. (2010). *Brittle Culm 12*, a dual-targeting kinesin-4 protein, controls cell-cycle progression and wall properties in rice. *Plant J* 63:312-328.
- Zhong, R., Burk, D.H., Morrison W Herbert, III, and Ye, Z.-H. (2002). A kinesin-like protein is essential for oriented deposition of cellulose microfibrils and cell wall strength. *Plant Cell* 14:3101-3117.
- Zhou, J.L., Qiu, J., and Ye, Z.H. (2007). Alteration in secondary wall deposition by overexpression of the Fragile Fiber1 kinesin-like protein in Arabidopsis. *Journal Of Integrative Plant Biology* 49:1235-1243.
- Zhu, C., and Dixit, R. (2011). Single molecule analysis of the Arabidopsis FRA1 kinesin shows that it is a functional motor protein with unusually high processivity. *Mol Plant* 4:879-885.

Zhu, C.J., and Jiang, W. (2005). Cell cycle-dependent translocation of PRC1 on the spindle by Kif4 is essential for midzone formation and cytokinesis. *Proc Nat Acad Sci USA* 102:343-348.

FIGURE LEGENDS

Figure 1. Homology among Kinesin-4 motors. The bar diagrams represent four Kinesin-4 motors: Gh KINESIN-4A, At KINESIN-4A/FRA1, At KINESIN-4C, and MmKIF4 from mouse. The motor domain is highlighted in tilted stripes, the neck domain in black, and coiled-coil domains in gray. GhKinesin-4A is most closely related to At KINESIN-4A/FRA1. Sequence identity and similarity (in parentheses) were given between highlighted regions in paired comparisons. Higher homologies are found in the motor domains than the rest between plant and animal Kinesin-4 motors.

Figure 2. Gh KINESIN-4A is associated with vesicle-like structures along cortical MTs. (A) Affinity purified antibodies detect the Gh KINESIN-4A polypeptide (arrowhead, lane 1) together with a degradation product (asterisk). Both bands are not detected after blocking the antibodies by the antigen. (B) Immunofluorescence of GhKinesin-4A and cortical MTs in a cotton fiber. Particles decorated by anti-Gh KINESIN-4A (arrows) are associated with cortical MTs aligned perpendicularly to the axis of fiber elongation. (C) Enlarged view of the boxed area in (B), showing close-view of punctate structures decorated by Gh KINESIN-4A (arrowheads) that are associated with cortical MTs.

Figure 3. Complementation of the *kinesin-4a* mutation. The *kinesin-4a* mutant exhibits dwarfed phenotype when compared to the wild-type. Upon the expression of the VisGreen-At KINESIN-4A-GFP fusion protein, this growth retardation phenotype is completely suppressed as demonstrated by three independent transformation lines.

Figure 4. Live-cell imaging of the VisGreen-At KINESIN-4A-GFP fusion in leaf epidermal cells. (A) The fusion protein appears in fluorescent particles at the cell cortex. (B) Time-averaged image represents the motile history of the fusion protein over 4 minutes. Arrows point at examples of processive movements. Arrowheads highlight the region used for Kymographic analysis in (D). (C) The fusion protein is only detected at the cortex but not in the interior part of the cell. (D) Kymograph analysis shows the motility over 4 minutes. Scale bar, 5 μm .

Figure 5. Motility of VisGreen-At KINESIN-4A-GFP along cortical MTs. The merged images have MTs in red, AtKinesin-4A in green. (A) Particles decorated by VisGreen-At KINESIN-4A-GFP are frequently associated with cortical MTs marked by mCherry-TUB6. Arrowheads highlight the region used for time-lapsed and Kymographic analyses. (B) Examples of motile (arrowheads) and immotile (asterisks) AtKinesin-4-decorated particles on a cortical MT. Time in seconds is indicated on the left. (C) Kymograph reporting the motility of both motile and immotile particles shown in (B) over 270 seconds. Scale bars, 5 μm (A) and 2.5 μm (B).

Figure 6. Distributions of KINESIN-4A motility and run-length. The mean values are shown with standard deviations and examined sample sizes. Dotted lines represent the trends derived from Gaussian fits. (A) Velocity frequencies of VisGreen-Kinesin-4A-GFP that moves along cortical MTs. (B) Distribution of the run length of VisGreen-

KINESIN-4A-GFP. (C) Frequency distribution of the cellulose synthase fusion GFP-CESA3. (D) The distribution of MT polymerization rates reported by the EB1b-GFP fusion.

Figure 7. Retardation of axial growth caused by the *kinesin-4a* and *kinesin-4c* mutations. (A) Rosette morphology of 23-day old seedlings of the wild-type control, the *kinesin-4a* single, and *kinesin-4a; kinesin-4b* as well as *kinesin-4a; kinesin-4c* double mutants. (B) Diameters of rosettes formed by the 18-32-day old seedlings of the aforementioned genotypes. (C) Inluorescences of 32-day old plants of the four genotypes. (D) Quantification of the inluorescence stem length in four different plants. (E) Fully developed siliques of the wild-type control, the *kinesin-4a* single, and *kinesin-4a; kinesin-4c* double mutants. (F) Numbers of seeds produced per silique in the wild-type control, the *kinesin-4a*, *kinesin-4b*, and *kinesin-4c* single mutants, as well as *kinesin-4a; kinesin-4b*, *kinesin-4b; kinesin-4c*, and *kinesin-4a; kinesin-4c* double mutants. Scale bars, 5 cm in (A) and (C) and 5 mm in (E).

Figure 8. Cell wall rigidity is higher during developmental time in *kinesin-4a; kinesin-4c* double mutants. (A) Apparent Young's Modulus values taken from cell walls perpendicular to the leaf surface for WT and *kinesin-4a; kinesin-4c* double mutant leaves. Data were collected from epidermal cells overlaying the developing midrib and bulked by age and genotype from 3-4 biological replicates. (B) All Apparent Young's Modulus data from all walls in the assessed area. WT data is shaded grey and *kinesin-*

4a; *kinesin-4c* in white. Means and medians are graphed on violin plots. Statistical groups in (A) are based on T-test P values of <0.001.

SUPPLEMENTAL FIGURE LEGENDS

Supplemental Figure 1. Phylogenetic analysis of Kinesin-4 motors. (A) The phylogeny analysis was carried out with the program PhyML (www.phylogeny.fr) based on the amino acid sequences of the kinesin motor domain. The maximum likelihood method was used. Branch support values were represented in percentages (%), and only values greater than 50% were displayed in the figure. The following kinesin proteins were included in the analysis: At KINESIN-4A/FRA1 (At5g47820), At KINESIN-4B (At3g50240) and At KINESIN-4C (At5g60930) are from *Arabidopsis thaliana*; Gh KINESIN-4A (KJ701508) is from cotton (*Gossypium hirsutum*); LOC_Os09g02650 and LOC_Os02g50910 from rice (*Oryza sativa*); PpKIN4-1a to -1e (Phypa_#437833, 438737, 432365, 453193, 441211) and PpKIN4-2a to -2c (Phypa_#447296, 433281, 446183) from *Physcomitrella patens*; and MmKIF4 (NP_032472) from mouse (*Mus musculus*). The motor domain of At KINESIN-12A (At4g14150; AF193767) from *A. thaliana* served as an outgroup in the analysis. (B) Sequence identity and similarity (parenthesis) between At KINESIN-4A and At KINESIN-4B and At KINESIN-4A and At KINESIN-4C in the motor domains as well as outside. In the diagrams, the motor domains are highlighted in yellow, neck in red, and coiled-coils in blue.

Supplemental Figure 2. The *kinesin-4a* mutation does not affect the motility of the cellulose synthase complex. (A) Representative single frame image of YFP-CESA6 from the control and *kinesin-4a* seedlings. Epidermal cells ~2 mm below the apical hook were imaged by confocal microscopy. Five-minute time averaged images show that CESA particles along linear tracks. Bar = 10 μ M. (B) Histograms of particle velocities. The mean velocity is 213 ± 45 in the wild type ($n = 1223$) and 196 ± 90 in *kinesin-4a* ($n = 1279$).

Supplemental Figure 3. KINESIN-4A does not associate with SmaCCs/MASCs. (A) No co-localization was observed in the merged image of GFP-Kinesin-4A and RFP-CSI1. Circles denote GFP-KINESIN-4A and RFP-CSI1 above background. Bar = 5 μ m. (B) GFP-KINESIN-4A and RFP-CSI1 show different dynamic behaviors. Time in seconds is indicated above the images. Bar = 1 μ m.

Supplemental Figure 4. Growth phenotypes exhibited by the *kinesin-4a*, *kinesin-4b*, and *kinesin-4c* mutants. While the *kinesin-4a* mutant shows dwarfed growth, the *kinesin-4b*, and *kinesin-4c* mutation do not cause a noticeable phenotype.

Supplemental Figure 5. KINESIN-4A and KINESIN-4C regulate trichome elongation. Reduced trichome height caused by the *kinesin-4a* mutation is enhanced by *kinesin-4c*.

Supplemental Figure 6. Determination of cell wall mechanics in the wild-type (WT) and *kinesin-4a; kinesin-4c* double mutant. (A) The WT and double mutant seedlings on agar plate. (B) Representative leaves dissected from the WT and double mutant. (C) AFM Apparent Young's Modulus maps (32x32 bit, 100umx50um grid). Each pixel represents the apparent Young's modulus from one nano indentation. Perpendicular cell walls appear more rigid due to geometry and a difference in the indentation geometry; they allow cell shapes to be discerned. The color scale is for all images.

SUPPLEMENTAL MOVIES

Supplemental Movie 1. Time-lapsed movie of VisGreen-At KINESIN-4A-GFP in epidermal cells shown in Figure 4.

Supplemental Movie 2. Time-lapsed movie of VisGreen-At KINESIN-4A-GFP and mCherry-TUB6 in the epidermal cell shown in Figure 5.

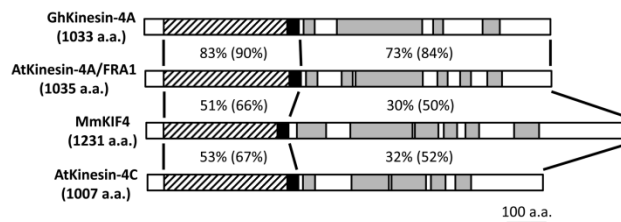


Figure 1. Homology among Kinesin-4 motors. The bar diagrams represent four Kinesin-4 motors: Gh KINESIN-4A, FRA1/At KINESIN-4A, At KINESIN-4C, and MmKIF4 from mouse. The motor domain is highlighted in tilted stripes, the neck domain in black, and coiled-coil domains in gray. GhKinesin-4A is most closely related to At KINESIN-4A/FRA1. Sequence identity and similarity (in parentheses) were given between highlighted regions in paired comparisons. Higher homologies are found in the motor domains than the rest between plant and animal Kinesin-4 motors.

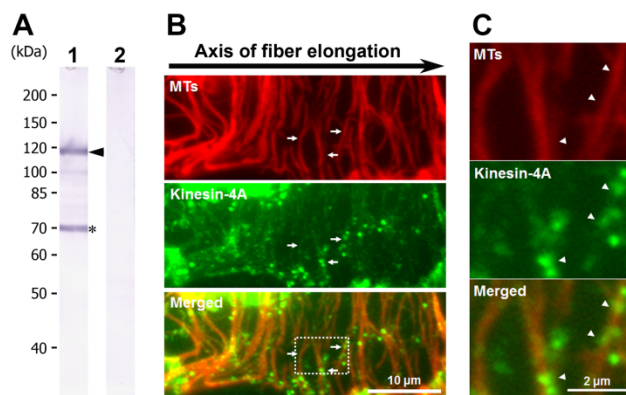


Figure 2. Gh KINESIN-4A is associated with vesicle-like structures along cortical MTs. (A) Affinity purified antibodies detect the Gh KINESIN-4A polypeptide (arrowhead, lane 1) together with a degradation product (asterisk). Both bands are not detected after blocking the antibodies by the antigen. (B) Immunofluorescence of GhKinesin-4A and cortical MTs in a cotton fiber. Particles decorated by anti-Gh KINESIN-4A (arrows) are associated with cortical MTs aligned perpendicularly to the axis of fiber elongation. (C) Enlarged view of the boxed area in (B), showing close-view of punctate structures decorated by Gh KINESIN-4A (arrowheads) that are associated with cortical MTs.

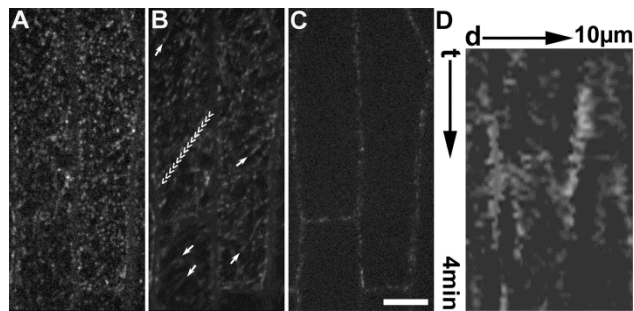


Figure 4. Live-cell imaging of the VisGreen-At KINESIN-4A-GFP fusion in leaf epidermal cells. (A) The fusion protein appears in fluorescent particles at the cell cortex. (B) Time-averaged image represents the motile history of the fusion protein over 4 minutes. Arrows point at examples of processive movements. Arrowheads highlight the region used for Kymographic analysis in (D). (C) The fusion protein is only detected at the cortex but not in the interior part of the cell. (D) Kymograph analysis shows the motility over 4 minutes. Scale bar, 5 μm .

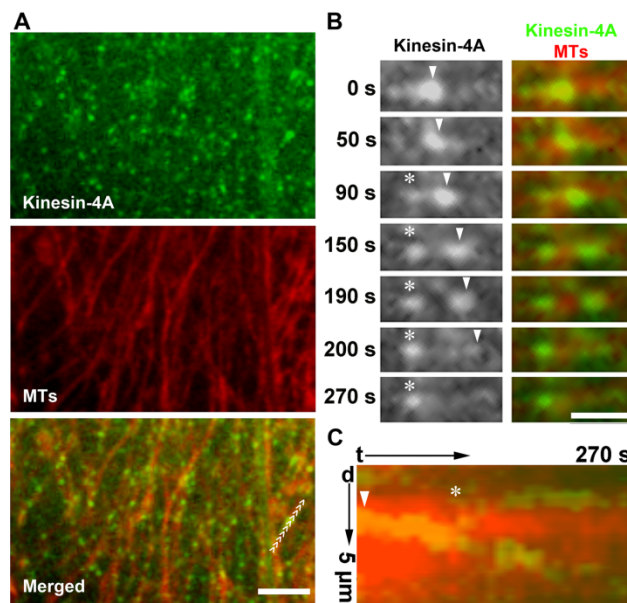


Figure 5. Motility of VisGreen-At KINESIN-4A-GFP along cortical MTs. The merged images have MTs in red, AtKinesin-4A in green. (A) Particles decorated by VisGreen-At KINESIN-4A-GFP are frequently associated with cortical MTs marked by mCherry-TUB6. Arrowheads highlight the region used for time-lapsed and Kymographic analyses. (B) Examples of motile (arrowheads) and immotile (asterisks) AtKinesin-4-decorated particles on a cortical MT. Time in seconds is indicated on the left. (C) Kymograph reporting the motility of both motile and immotile particles shown in (B) over 270 seconds. Scale bars, 5 μm (A) and 2.5 μm (B).

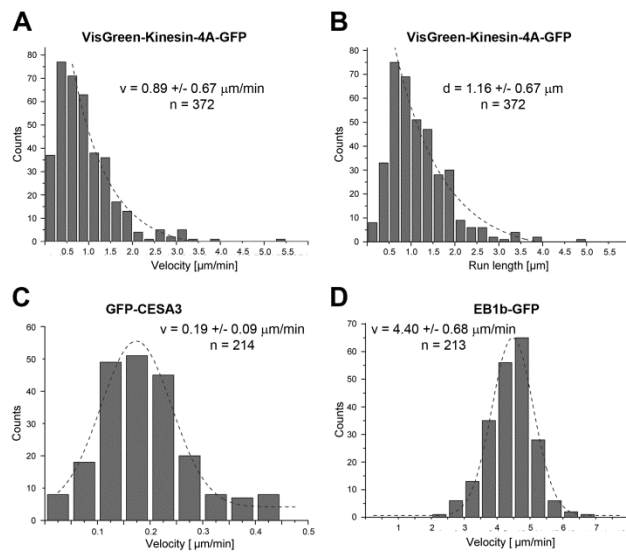


Figure 6. Distributions of KINESIN-4A motility and run-length. The mean values are shown with standard deviations and examined sample sizes. Dotted lines represent the trends derived from Gaussian fits. (A) Velocity frequencies of VisGreen-Kinesin-4A-GFP that moves along cortical MTs. (B) Distribution of the run length of VisGreen-KINESIN-4A-GFP. (C) Frequency distribution of the cellulose synthase fusion GFP-CESA3. (D) The distribution of MT polymerization rates reported by the EB1b-GFP fusion.

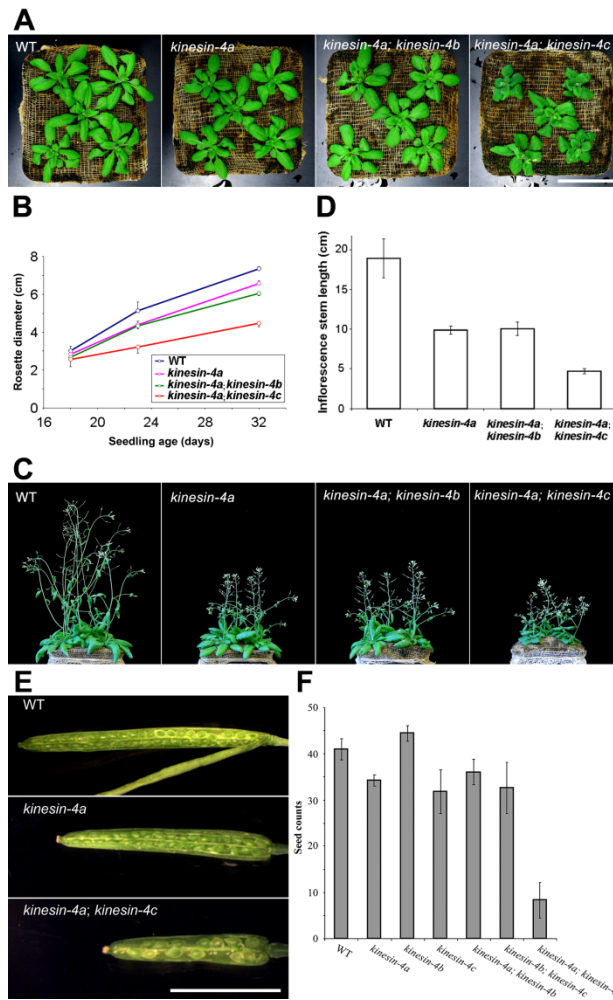


Figure 7. Retardation of axial growth caused by the *kinesin-4a* and *kinesin-4c* mutations. (A) Rosette morphology of 23-day old seedlings of the wild-type control, the *kinesin-4a* single, and *kinesin-4a*; *kinesin-4b* as well as *kinesin-4a*; *kinesin-4c* double mutants. (B) Diameters of rosettes formed by the 18-32-day old seedlings of the aforementioned genotypes. (C) Inflorescences of 32-day old plants of the four genotypes. (D) Quantification of the inflorescence stem length in four different plants. (E) Fully developed siliques of the wild-type control, the *kinesin-4a* single, and *kinesin-4a*; *kinesin-4c* double mutants. (F) Numbers of seeds produced per silique in the wild-type control, the *kinesin-4a*, *kinesin-4b*, and *kinesin-4c* single mutants, as well as *kinesin-4a*; *kinesin-4b*, *kinesin-4b*; *kinesin-4c*, and *kinesin-4a*; *kinesin-4c* double mutants. Scale bars, 5 cm in (A) and (C) and 5 mm in (E).

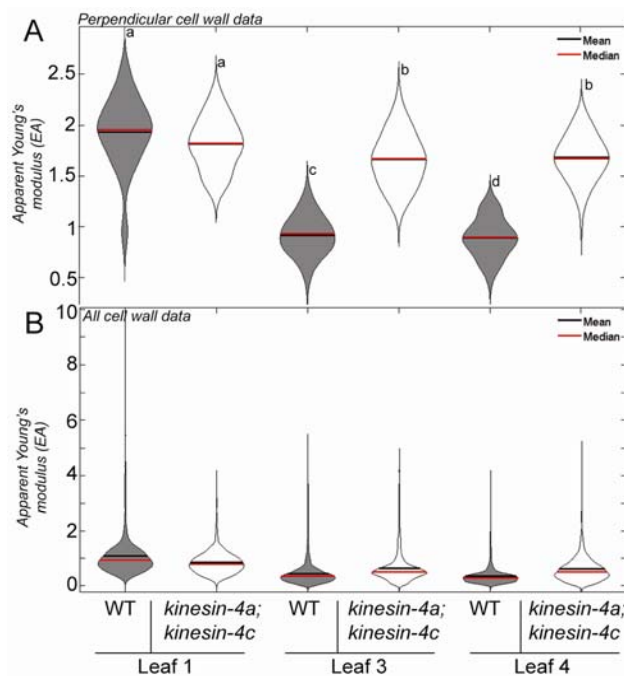


Figure 8. Cell wall rigidity is higher during developmental time in *kinesin-4a; kinesin-4c* double mutants. (A) Apparent Young's Modulus values taken from cell walls perpendicular to the leaf surface for WT and *kinesin-4a; kinesin-4c* double mutant leaves. Data were collected from epidermal cells overlaying the developing midrib and bulked by age and genotype from 3-4 biological replicates. (B) All Apparent Young's Modulus data from all walls in the assessed area. WT data is shaded grey and *kinesin-4a; kinesin-4c* in white. Means and medians are graphed on violin plots. Statistical groups in (A) are based on T-test P values of <0.001.